Electronic Supplementary Information for

Implications for New Particle Formation in Air of the Use of Monoethanolamine in Carbon Capture and Storage

Véronique Perraud,* Kanuri Roundtree, Patricia M. Morris, James N. Smith* and Barbara J. Finlayson-Pitts

The supporting information (26 pages) contains text covering additional details on the experimental methods as well as 15 figures (S1-S15).
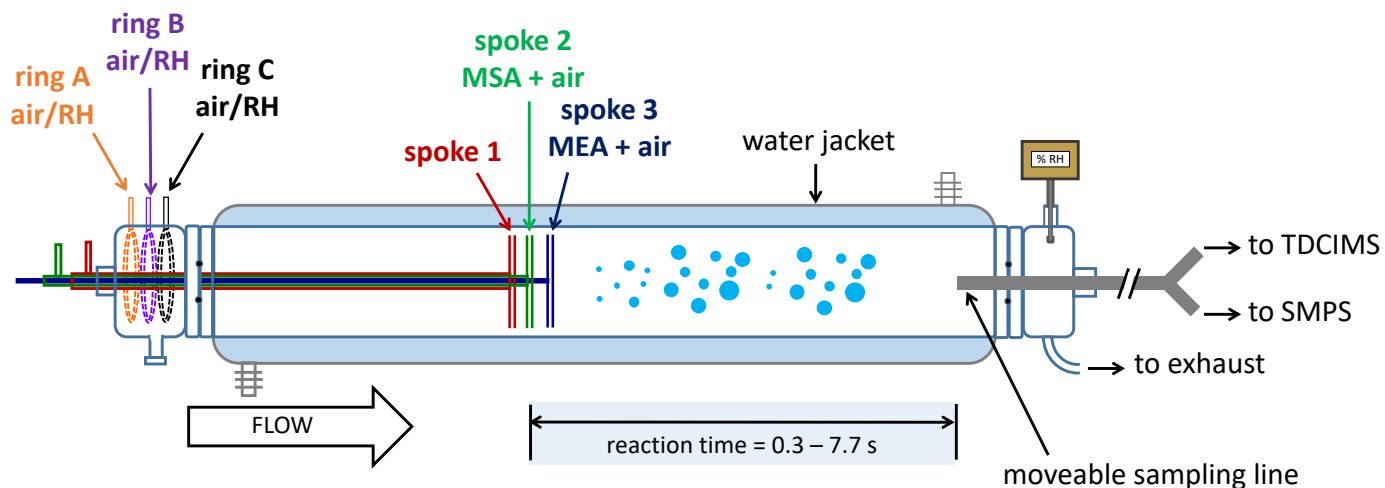
Flow reactor diagram

Figure S1. Diagram of the 1-m borosilicate flow reactor (adapted from Perraud et al.[1]) for the MSA+MEA experiments. Flows were distributed as follows: ring A, 4.3 or 8.5 L min^{-1} (either dry or humidified air); ring B, 4.2 or 8.5 L min^{-1} (either dry or humidified air); ring C, 0 or 4.3 L min^{-1} (either dry or humidified air); spoke 1 had no flow; spoke 2, ~1 L min^{-1} (mixture of MSA flow and clean air); spoke 3, ~1 L min^{-1} (mixture of MEA flow and clean air). All the flows were controlled by high-precision mass flow controllers (Alicat or MKS) and were checked with a flow meter (Sensidyne; Gilibrator 2) periodically. The reaction times at which measurements were taken ranged from 0.5 to 7.7 s (total flow ~10.7 L min^{-1}) or 0.3 to 4.5 s (total flow ~23.4 L min^{-1}).

Text S1. Gas phase reactant concentration determination.

(a) MSA sampling and analysis: The flow of gas phase MSA exiting the trap (53, 107, or 216 ccm) was sampled through a 33 mm diameter Durapore filter (Millex-HV, 0.45 µm pore size) for 10 min. Immediately after sampling, the filter was extracted using 10 mL of nanopure water and the extract was stored at room temperature prior to analysis by UPLC-ESI-MS(-). Each measurement was carried out in triplicate. For each sample, a 5 µL aliquot was analyzed using an UPLC-PDA-MS platform (Waters) equipped with an Acquity UPLC system (including a quaternary pump, an autosampler, a column manager and a photodiode array detector) coupled to a Xevo TQD triple quadrupole mass spectrometer. An Aquity UPLC BEH C18 column (2.1 x 50 mm, 1.7 µm thickness; Waters) fitted with a BEH C18 (2.1 x 5.0 mm; Waters) guard column maintained at 50°C was used for the separation. The isocratic mobile phase (400 µL min^{-1}) was composed of 95% of a 0.2% acetic acid (Optima, LC-MS grade, Fisher) aqueous solution (18.2 MΩ-cm nanopure water) combined with 5% LC-MS grade methanol (Optima, Fisher). The sample exiting the analytical column was introduced into the mass spectrometer using an electrospray ionization source (ESI) set in negative ion mode, with the following parameters: capillary voltage, 2.0 kV; cone voltage, 40 V; desolvation temperature, 500°C, desolvation gas flow rate, 1000 L hr^{-1}; source temperature, 120°C. The analysis was performed using a multiple reaction monitoring (MRM) method following the m/z 95 ($CH_3SO_3^-$) => 80 (SO_3^-) transition that is specific to MSA, with a collision energy of 16 eV. The data were acquired using MassLynx (Waters) and processed using TargetLynx (Waters).

(b) MEA/MA sampling and analysis: The flow of gas phase amine (MEA or MA) exiting the trap was sampled using custom-built cation exchange resin cartridges[2] for 20 or 40 min. Prior to the first sampling, the cartridges were first cleaned and conditioned by flushing them ten times with the extraction solution which is a 50 mM oxalic acid solution in nanopure water. The solution was prepared daily by dissolving 9 g of oxalic acid (Sigma Aldrich, 98%) into 2 L of nanopure water. Immediately after sampling, the cartridges were extracted sequentially three times with 10 mL of the extraction solution. The three extracts were collected and analyzed separately. The amines were mostly present in the first extract (recovery 93-100%) but the additional extractions were performed to ensure full recovery and to ensure the cartridge was clean for the next sampling. The extracts (injection volume 25 uL) were analyzed using a Dionex IC1100 (ThermoScientific) ion chromatography system equipped with a CERS500 4 mm suppressor and a Dionex GC16 (5 x 50 mm) guard column coupled to an IonPac CS16 (5 x 25 mm) analytical column. The separation of the amines was achieved using an isocratic eluent composed of a 50 mM oxalic acid in nanopure water with a flow rate of 1 mL min^{-1}, and a column temperature maintained at 40°C. The amines were detected by conductimetry.

Calibration curves for MEA and MA were obtained using monoethanolamine hydrochloride (MEA-HCl; Sigma Aldrich, > 99.0%) and methylamine hydrochloride (MA-HCl; Aldrich; >98%) standard solutions in water, respectively. Data were acquired using Chromeleon (ThermoScientific, version 7.2.10). An example of a chromatogram obtained from a cartridge extract is presented in Fig. S2 and shows no additional measurable ammonia in the extract compared to the blank cartridge. The gas phase concentration of MEA was determined to be 164 ± 19 ppb out of the trap (n = 22; one standard variation), while the concentration of MA was 1.2 ± 0.2 ppm (n = 9; one standard variation).
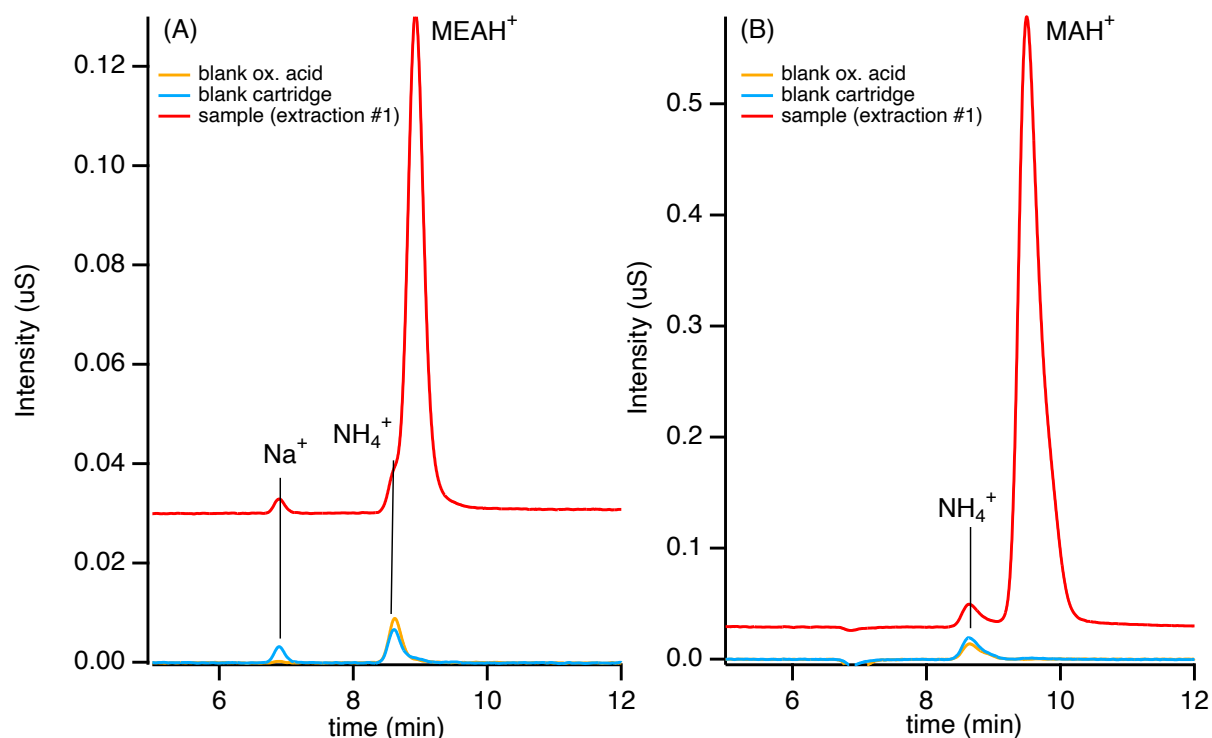
Figure S2. IC chromatograms of a cartridge extract (red trace) compared to a blank cartridge (blue trace) and the extraction solution (50 mM oxalic acid in nanopore water; orange trace) taken from (A) the MEA trap and (B) for the MA trap. The ammonia present in the extract originates from small amounts of ammonia present in the extraction solution.

Text S2. Particle transmission determination

The total particle transmission efficiency through the sampling lines as a function of particle

diameter (Fig. S3) were determined using a combination of measurements and simulation.

Exiting the flow tube reactor, the particles first traveled through a 142 cm long straight stainless

steel sampling line (0.64 cm O. D.). This tube is moved along the centerline of the FT to vary

reaction times. The total flow rate through the sampling line was either 3.5 L min^{-1} or 4.8 L

min^{-1} corresponding to the sum of the scanning mobility particle sizer (SMPS, 1.5L min^{-1}) and

the TDCIMS flows (either 2.0 L min^{-1} or 3.3 L min^{-1}). The particle transmission efficiency

through this sampling line was estimated using the particle loss calculator tool developed by von

der Weinder et al.[3] using a density of 1 g cm^{-3} and, the loss was calculated to be minimal for particles with diameter larger than 4 nm (> 80% particle transmission; red trace). The end of the sampling line was terminated by a y-shaped connector to split the flows between the TDCIMS and the SMPS. Sampling from the y-connector to the SMPS was initially conducted using a 117 cm long flexible stainless steel bellows attached to the FT sampling line. As described below, the rough walls of the bellows resulted in significant particle loss and was later replaced with a smooth bore 84 cm long aluminum tube. Comparing the two size distributions, a drastic loss of nanoparticles was observed when the bellows were used, and particle loss was experimentally determined by taking the ratio of particle concentrations measurements using the bellows to the particle concentrations measured with the straight shorter aluminum line (blue squares). To assess the total particle transmission efficiency through the entire sampling line from the FT to the inlet of the SMPS, the particle loss calculator was first used to estimate the losses through the FT sampling line (red trace) and then through the smooth bore aluminum line (green trace) connecting the sampling line to the SMPS. The total particle transmission efficiency through the sampling lines from the FT to the inlet of SMPS was then defined as the product of all individual particle transmission efficiencies (black trace). For example, as illustrated in Fig. S4, for a particle diameter of 6 nm, the particle transmissions are 0.88 (FT sampling lines), 0.86 (aluminum smooth bore line) and 0.44 (correction from bellows to aluminum line) respectively for a TDCIMS inlet flow of 2.0 L min^{-1}, yielding a total particle transmission efficiency through the entire sampling line of $0.88 \times 0.86 \times 0.44 = 0.33$. Subsequently, all results presented in this work have been normalized for the total particle transmission efficiency.
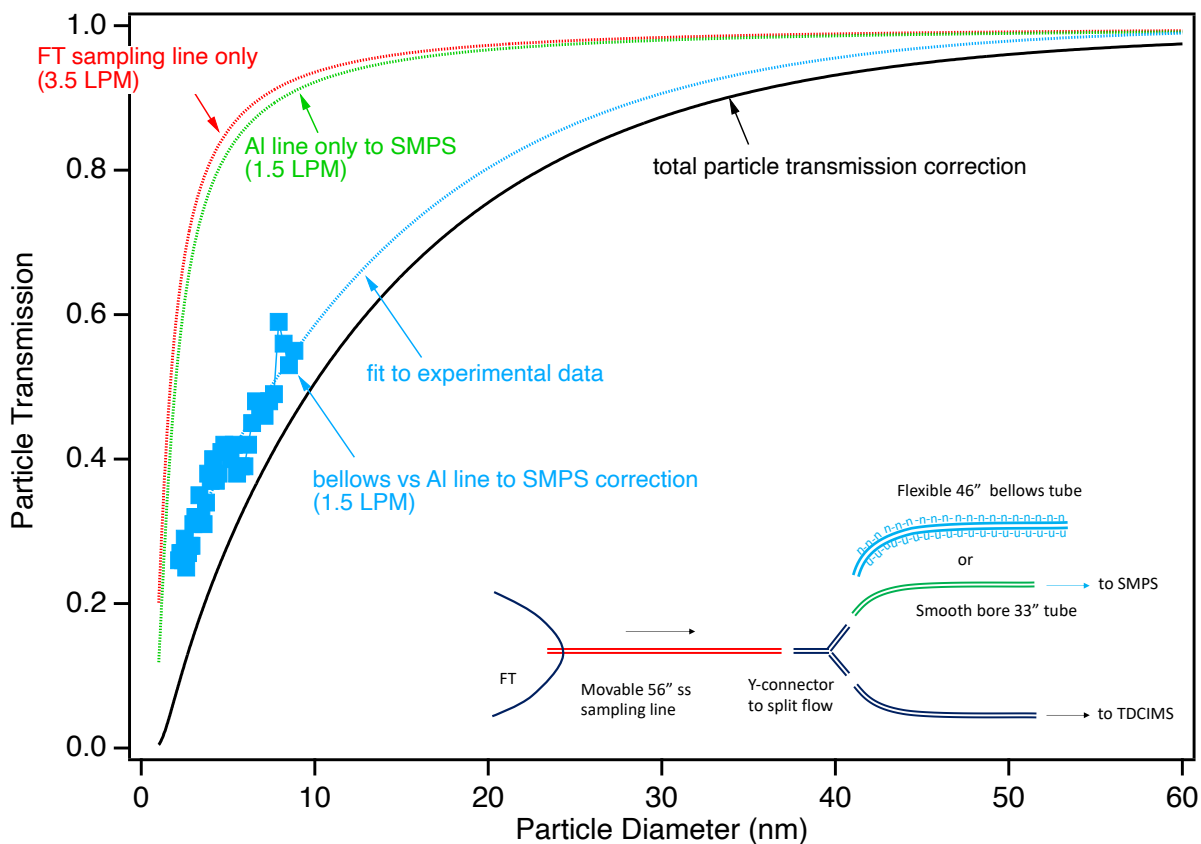
Figure S3. Example of determination of the particle transmission through the sampling lines to the SMPS inlet for a TDCIMS inlet flow of 2.0 L min⁻¹. Red and green lines represent simulated[3] particle transmission through the flow tube sampling line (3.5 L min⁻¹) and through the aluminum smooth bore line to the SMPS (1.5 L min⁻¹), respectively. Blue squared data points correspond to experimentally determined particle transmission correction (bellows vs aluminum line to the SMPS, 1.5 L min⁻¹). The blue line corresponds to the fit to the experimental data. The black line represents the final total particle transmission through the sampling line train to the SMPS accounting for all corrections. (LPM corresponds to L min⁻¹; ss, stainless steel)
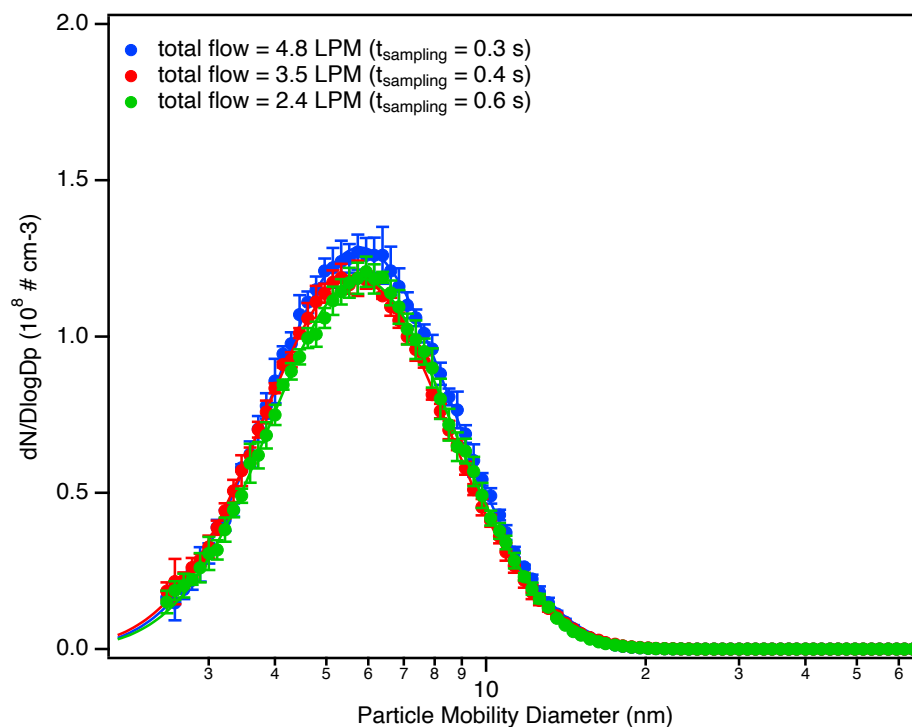
Figure S4. Size distributions of particles measured by the SMPS for the MSA (6.1 ppb) + MEA (3.3 ppb) reaction at different flow rates and residence times in the sampling line. All measurements were conducted at 0.5 s reaction time under dry conditions, but a similar result was obtained for all reaction times. Size distributions are all corrected for particle losses through the sampling lines (see Text S2 above). $t_{sampling}$ refers to the extra residence time the particles have in the flow tube sampling line, over and above the reaction time in the flow tube.

Stability of the size distributions measured from the MSA+MEA system
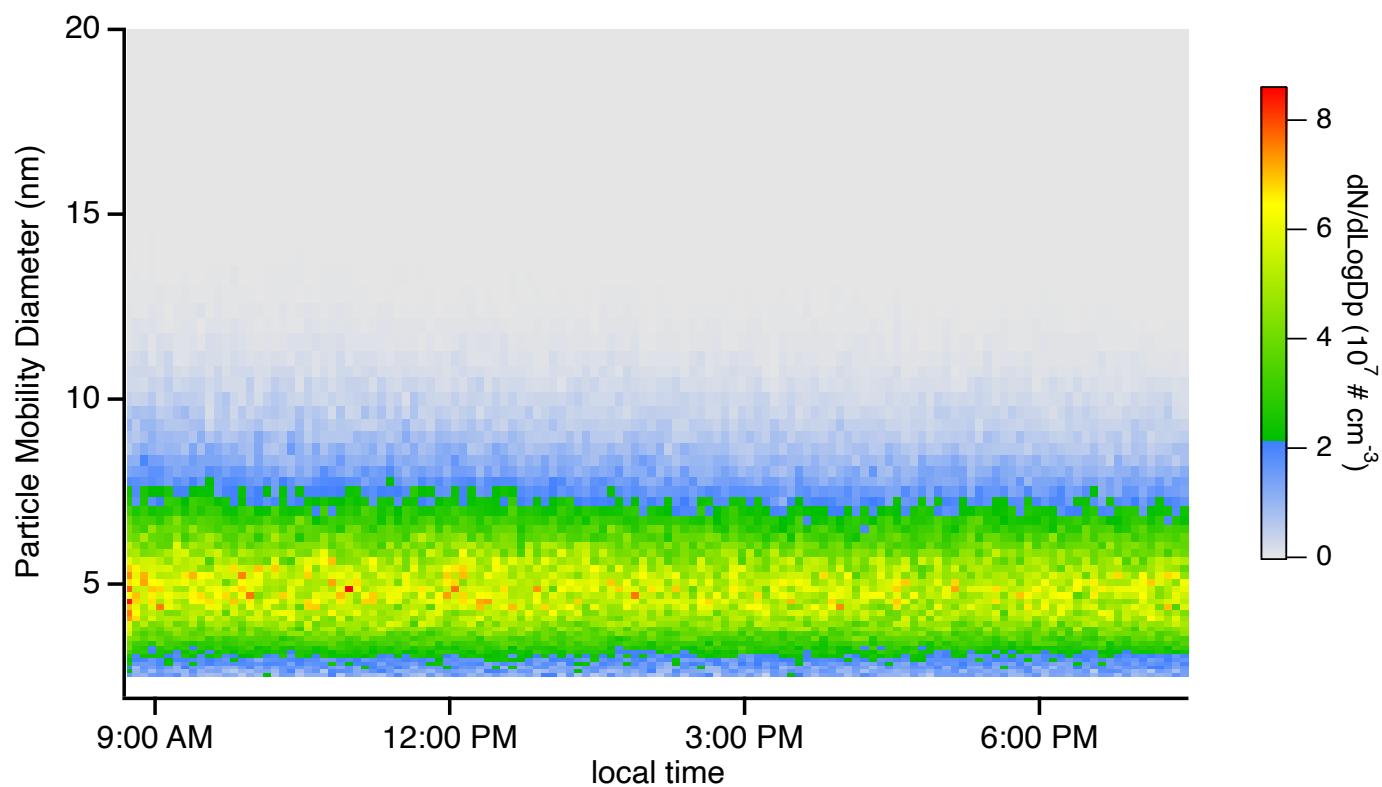

Figure S5. Stability of the size distribution of particles measured by the SMPS for the MSA (0.68 ppb) + MEA (1.4 ppb) reaction system. The measurement was conducted at 4.5 s reaction time under dry condition. Size distributions are corrected for particle losses through the sampling lines (see Text S2 above).
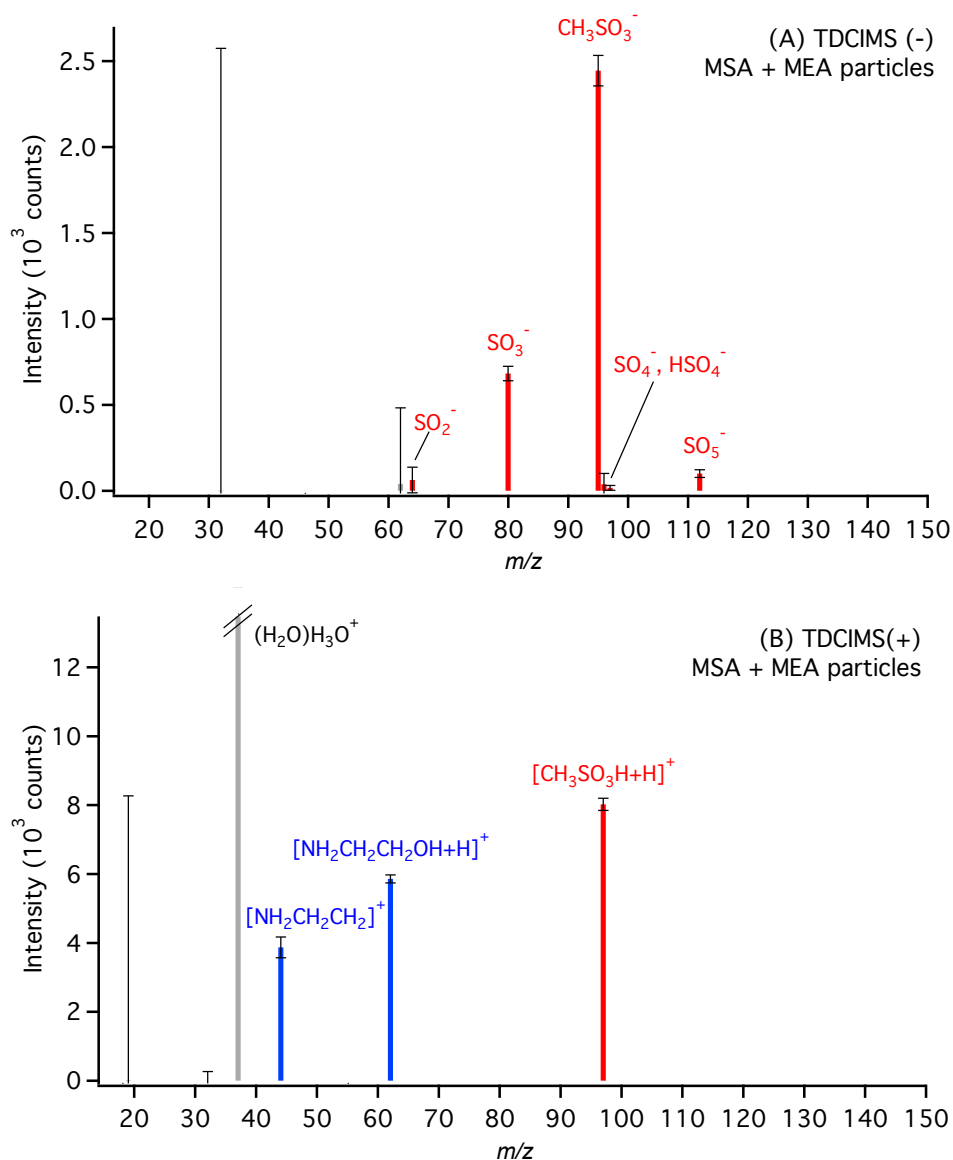
Details of the TDCIMS analysis

Figure S6. Representative mass spectra of ion abundance observed for MSA-MEA particles collected at 4.5 s reaction time in (A) negative ion mode and (B) positive ion mode (volume mean diameter 6.8 nm; collection time, 120 s; [MSA] =0.68 ppb; [MEA] = 1.5 ppb). The red traces correspond to ions observed for MSA while the blue traces are for MEA. Note these are not raw MS spectra, but rather they represent the distribution of the ions observed for each species (i.e. all the other ions have been omitted for clarity). The observed MS spectra were not dependent on the reactant concentrations (i.e. the same ions were observed for all [MSA] concentrations investigated), but the signal intensity measured for each ion was proportional to the mass of nanoparticle collected. The grey bars represent the reagent ions.
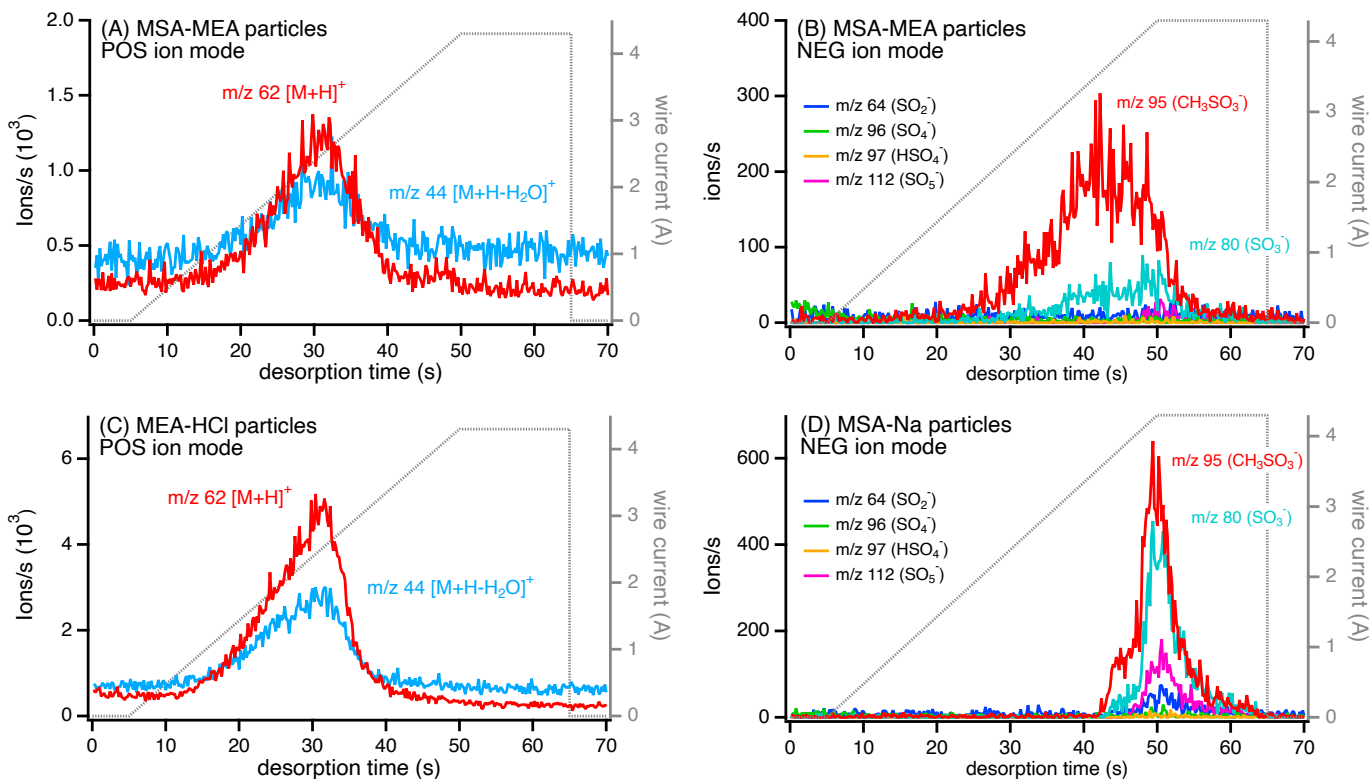
Figure S7. Representative ion desorption profiles for (A) MEA and (B) MSA present in 6 nm MSA-MEA particles collected from the flow reactor (collection time = 120 s), (C) MEA present in 15 nm atomized MEA-HCl particles (collection time = 240 s) and (D) MSA present in 15 nm atomized MSA-Na particles (collection time = 240 s). In all graphs, the grey line corresponds to the wire current.

Text S3. TDCIMS analysis cycle description: The TDCIMS method has been described in detail previously.[1,4-6] Briefly, sampled particles were charged and size-selected using two unipolar chargers and radial differential mobility analyzers operating in parallel. Particles were then electrostatically collected on a Pt wire by the application of a DC voltage of 3.5 kV. After collection for 10-1200 sec, the Pt wire was translated into the ion source where it was resistively heated by the application of a power-controlled AC current from room temperature to an estimated temperature of ~600°C for a duration of 70 s (corresponding to a wire current of 4.30

A) to desorb the particle components. The desorbed species were then ionized via chemical ionization using ions generated by a radioactive source (^{210}Po; NRD). Following ionization, each species was analyzed by a high-resolution time-of-flight mass analyzer (TOF mass analyzer, Tofwerk AG). Prior to each measurement, the wire was resistively heated at the maximum wire current of 4.30 A for 30 s to clean any residue left on the wire, followed by a cool down step (~30 s) to room temperature. Each collection cycle (cleaning/cooldown/ collection/analysis) was followed by a background cycle during which no collection voltage was applied to the Pt wire.

Text S4. Determination of the TDCIMS collection efficiency. An "exhaust SMPS" consisting of a ^{210}Po bipolar neutralizer, a nano-differential mobility diameter (nano-DMA; model 3085, TSI, Inc.) and an ultrafine condensation particle counter (UCPC; model 3776, TSI, Inc.) was used to detect the particles downstream of the TDCIMS inlet. The ^{210}Po bipolar neutralizer used in these studies was developed by the Particle Technology Lab (PTL) at the University of Minnesota as described in Jiang et al.[7] The exhaust SMPS measured the size distribution over the mobility range of 2.5 to 24 nm using a recirculating sheath air flow rate of 10 L min^{-1} and an aerosol flow rate of 1.5 L min^{-1}. This was used to determine the particle mean volume diameter of the collected particles, which is calculated by taking the difference between the distribution of the particles during background (i.e. when no voltage is applied to the Pt wire) and that of the particles during collection, and estimating the volume mean diameter (Fig. S8). A second UCPC (model 3025; TSI Inc.) located again downstream of the collection wire was used to determine the total particle concentration collected from the difference in concentration during background and collection runs; this measurement was used to assess the size-dependent collection efficiency of the TDCIMS for each diameter selected (Fig. S9).
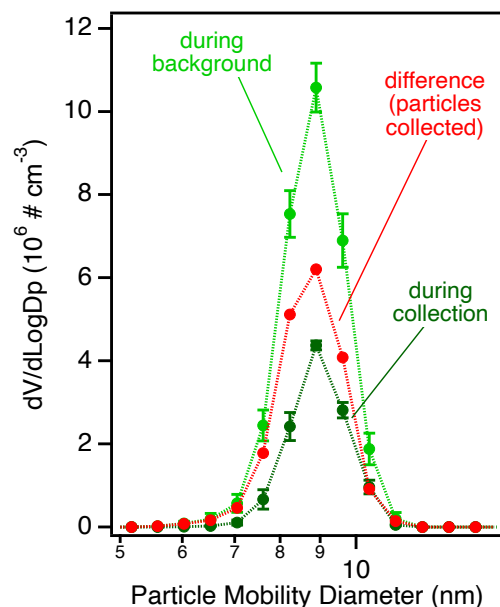
Figure S8. Example of a volume-based size distribution of MSA-MEA particles taken by the "exhaust" SMPS (i.e. detecting particles that are not collected by the Pt wire) for rDMA voltage = 110V (corresponding to a measured volume-based mean mobility diameter of 9 nm). The experimental data correspond to averages of at least two scans (error bars represent one standard deviation).
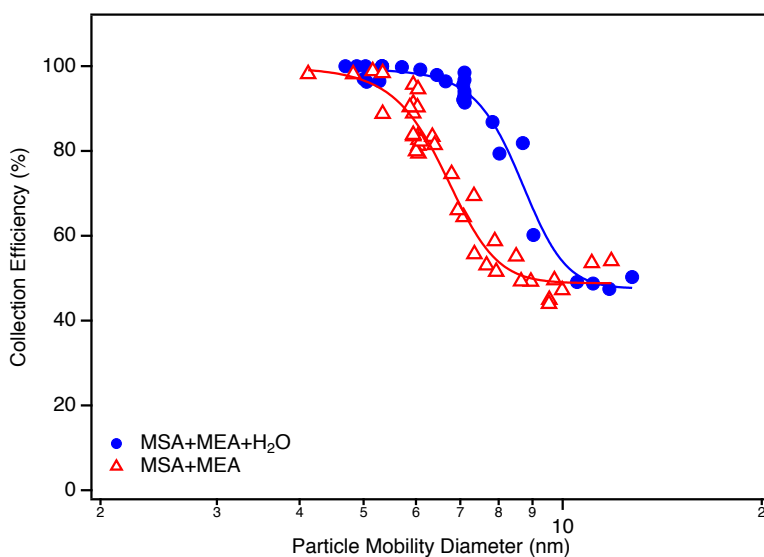

Figure S9. Experimentally determined TDCIMS collection efficiency for the MSA+MEA system (dry conditions; red trace) and the MSA+MEA+H_2O system (52% RH; blue trace). The TDCIMS was operated in high resolution mode with 1 L min^{-1} inlet flow and 10 L min^{-1} sheath air flow for each radial inlet DMA. For each data point, the particle mobility diameter corresponds to a volume mean diameter measured with the exhaust SMPS.

Text S5. TDCIMS calibration and acid/base molar ratio determination. Three or four specific ions present in all mass spectra were chosen in each polarity to mass calibrate each spectrum. In negative ion mode, these calibration ions were m/z 31.99 (O_2^-, reagent ion) as well as Cl^- ion at m/z 34.97 and NO_3^- at m/z 61.99 that were always present in the background. In the positive ion mode, these calibration ions were m/z 19.02 (H_3O^+, reagent ion) as well as N_2H^+ at m/z 29.01, and two siloxane peaks present at m/z 297.08 $[(CH_3SiCH_3O)_4+H]^+$ and 371.10 $[(CH_3SiCH_3O)_5+H]^+$. From each acquired mass spectrum, the desorption profile (i.e. intensity as a function of desorption time) for each ion of interest is extracted (Fig. S7). The desorption profiles are then processed following these steps to obtain a total background-subtracted integrated signal for each ion of interest: (1) the signal intensity for each ion is scaled to the reagent ion on a point-to-point basis over the entire desorption profile, and corrected for baseline; (2) the signal intensity is then integrated over a defined period of the desorption time; (3) the signal intensities of each ion for one given species (MSA or MEA) are summed; (4) the signal is normalized to an average reagent ion signal ($I^{reference}$ = 1.9× 10^4 ions/s for O_2^- and 1.1× 10^5 ions/s for H_3O^+) measured during calibration to account for day-to-day variability; and lastly (5) the corrected integrated signal intensity measured during a clean air sample is subtracted from that obtained during a collection to account for any residual signal from the system to yield a total signal intensity for negative ion mode (MSA) and positive ion mode (MEA) as:

$$(NEG\ signal) = \left(\sum neg\ ions(MSA)^{sample} \times \frac{I_{O_2^-}{}^{sample}}{I_{O_2^-}{}^{reference}} \right) - \left(\sum neg\ ions(MSA)^{cleanair} \times \frac{I_{O_2^-}{}^{cleanair}}{I_{O_2^-}{}^{reference}} \right) \quad (1)$$

$$(POS\ signal) = \left(\sum pos\ ions(MEA)^{sample} \times \frac{I_{H_3O^+}{}^{sample}}{I_{H_3O^+}{}^{reference}} \right) - \left(\sum pos\ ions(MEA)^{cleanair} \times \frac{I_{H_3O^+}{}^{cleanair}}{I_{H_3O^+}{}^{reference}} \right) \quad (2)$$

The signal for each polarity is thus used to estimate the acid/base molar ratio using equation (3) below:

$$\frac{acid}{base} \, molar\ ratio = \frac{(NEG\ signal)}{(POS\ signal)} \times \frac{total\ vol.\ pos\ coll.(s)}{total\ vol.neg\ coll.(s)} \times \frac{1}{\left(\frac{acid}{base}\ calibration\right)} \qquad (3)$$

where $\frac{acid}{base} \, calibration$ represent the calibrated acid/base molar ratio defined from an external

calibration using reference particles as described below, and accounting for the total volume of

particles collected (in cm^3) for each polarity as follows:

$$total\ vol.\ coll.(s) = \left(\frac{4}{3} \times \pi \times \left(\frac{d_{vol.}(nm)}{2} \times 10^{-7} \frac{cm}{nm}\right)^3\right) \times \left(N_{coll.} - N_{bkgd}\right) \times wire\ flow\left(\frac{cm^3}{s}\right) \times coll.\ time(s) \qquad (4)$$

Where $d_{vol}(nm)$ is the volume-based mean mobility diameter, $N_{coll.}$ and N_{bkgd} are the total particle

concentration measured with the UCPC located at the exhaust of the TDCIMS inlet region

during a collection or a background (no voltage applied on the Pt wire) scan respectively.

To determine the relative ionization efficiency of MSA versus MEA, reference salt

particles were generated using a constant output atomizer (TSI, Inc.; model 3076). Aqueous

solutions of sodium methanesulfonate (MSA-Na; 98%; Aldrich) and monoethanolamine

hydrochloride (MEA-HCl; ≥ 99%; Sigma Aldrich) were atomized separately using dry clean air

(32 psi) as the carrier gas. The flow exiting the atomizer was 1.7 L min^{-1} and passed through a

Nafion^{TM} drier (FC125-240-5MP-02; PermaPure) with 10 L min^{-1} drying air followed by a

diffusion drier containing molecular sieve (type 13X, Kurt J. Lesker and ACROS). The particles

were neutralized using a ^{210}Po bipolar neutralizer (NRD LLC; model P-2021) before being

diluted with an additional 3 to 5 L min^{-1} of dry clean air. Size distributions were measured using

the SMPS operated in high flow mode with an aerosol flow rate of 1.5 L min^{-1} and a sheath air

flow rate of 15 L min^{-1}. Typical representative size distributions for the atomized particles are

presented in Fig. S10. Particles were also sampled using the TDCIMS operating under high and low resolution to quantify MSA and MEA. For these measurements, particles with volume mean diameter ($d_{vol.}$) ranging from 15 to 17 nm were sampled. These were the smallest particles that could be sampled based on the size distribution generated. To estimate the total mass collected, the effective density (ρ_{eff}) for each set of particles was first determined using a tandem CPMA-SMPS approach.[8] Briefly, the atomized reference particles were first mass-selected using a centrifugal particle mass analyzer (CPMA, Cambustion, Ltd) and subsequently classified using the SMPS operating with a 0.3 L min^{-1} aerosol flow rate and either a 3 or a 15 L min^{-1} sheath air flow rate. Effective density (ρ_{eff}) for particles covering the range 20 – 200 nm were 1474 ± 13 kg m^{-3} for MSA-Na, 1136 ± 26 kg m^{-3} for MEA-HCl.[8] The total mass collected ($m_{coll.}$) was then derived as:

$$m_{part.}(\mu g) = \left(\frac{4}{3} \times \pi \times \left(\frac{d_{vol.}(nm)}{2} \times 10^{-7} \frac{cm}{nm}\right)^3\right) \times \left(\rho_{eff}\left(\frac{kg}{m^3}\right) \times 10^3 \frac{g}{kg} \times 10^{-6} \frac{m^3}{cm^3}\right) \times 10^6 \frac{\mu g}{g} \qquad (4)$$

$$m_{coll.}(pg) = m_{part.}(\mu g) \times \left(N_{coll.} - N_{bkgd}\right) \times wire\ flow\left(\frac{cm^3}{s}\right) \times coll.time(s) \times 10^6 \frac{pg}{ug} \qquad (5)$$

The wire flow was comprised of the inlet flow (3.3 L min^{-1} or 2 L min^{-1}) and the ultrahigh purity nitrogen sheath air flow (1.25 L min^{-1}). Calibration curves for each species (Fig. S11) were plotted with the background-subtracted integrated signal as a function of the total number of moles collected:

$$(NEG\ ion\ signal) = slope(MSA) \times \left(\frac{m_{coll.}(MSANa)}{MW(MSANa)}\right) \qquad (6)$$

$$(POS\ ion\ signal) = slope(MEA) \times \left(\frac{m_{coll.}(MEAHCl)}{MW(MEAHCl)}\right) \qquad (7)$$

Thus, the

acid/base reference calibrated molar ratio can be defined as:

$$\frac{acid}{base}\ calibration = \frac{slope(MSA)}{slope(MEA)} \tag{8}$$

The slopes are for MSA 3.5×10^{17} counts mole^{-1}, and for MEA 3.9×10^{17} counts mole^{-1},
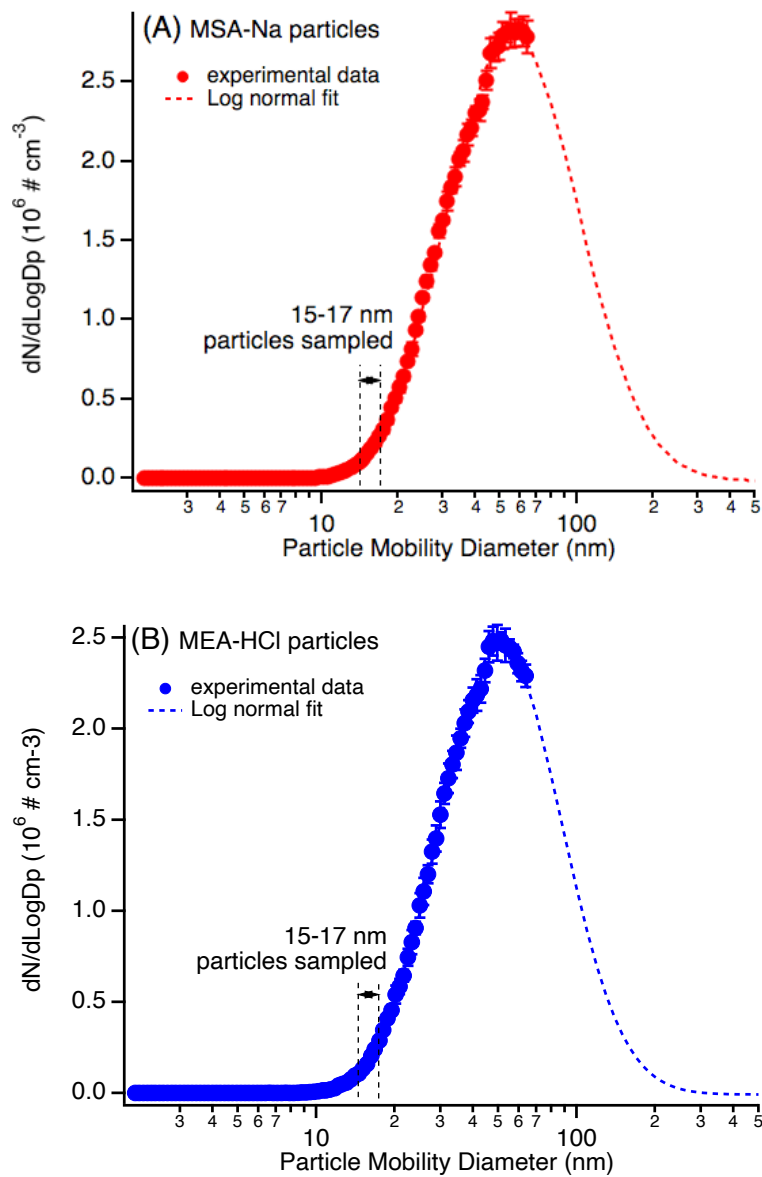
yielding a reference molar ratio of 0.89.

Figure S10. Typical size distributions of (A) MSA-Na and (B) MEA-HCl atomized reference particles. The SMPS was operated with an aerosol flow rate of 1.5 L min^{-1} and a sheath air flow rate of 15 L min^{-1}, resulting in a maximum mobility diameter of 64 nm.
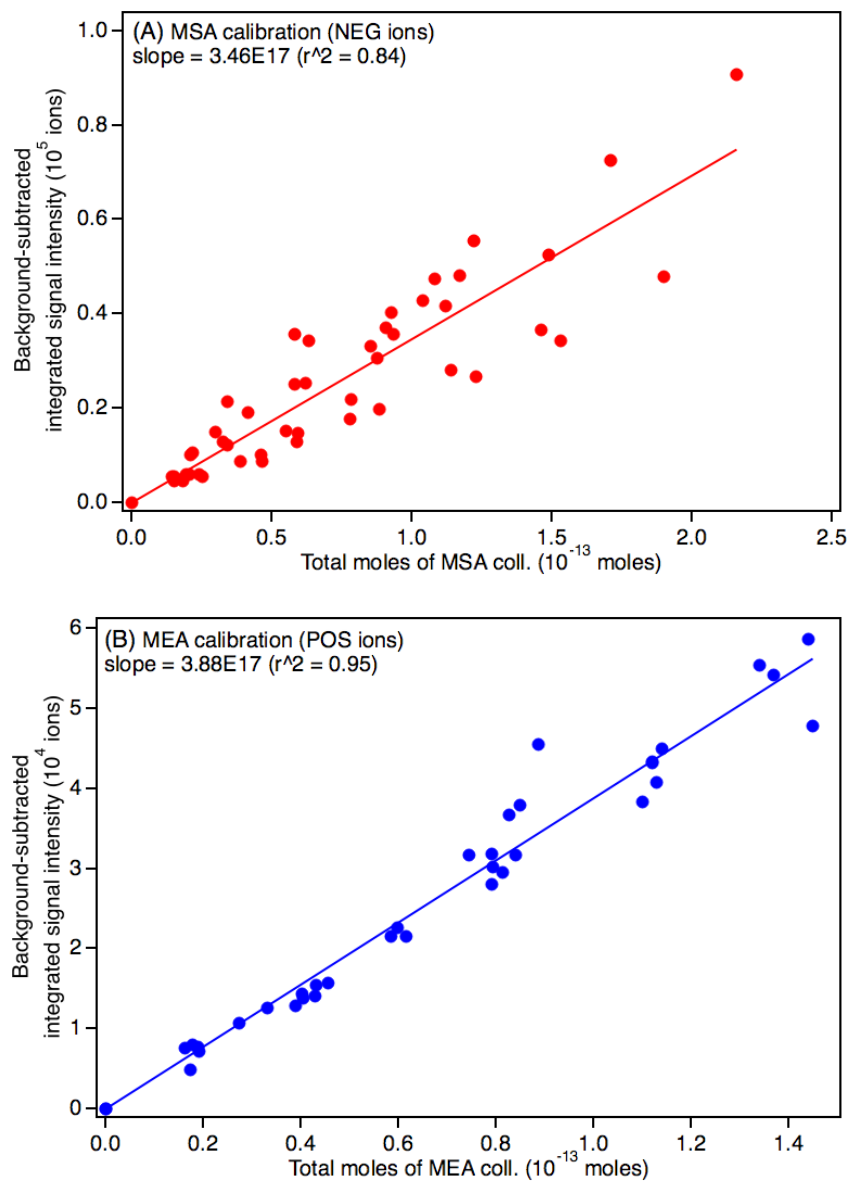
Figure S11. Calibration curves for (A) MEA and (B) MSA obtained from MEA-HCl and MSA-Na atomized particles, respectively, with diameters ranging from 15 to 17 nm.

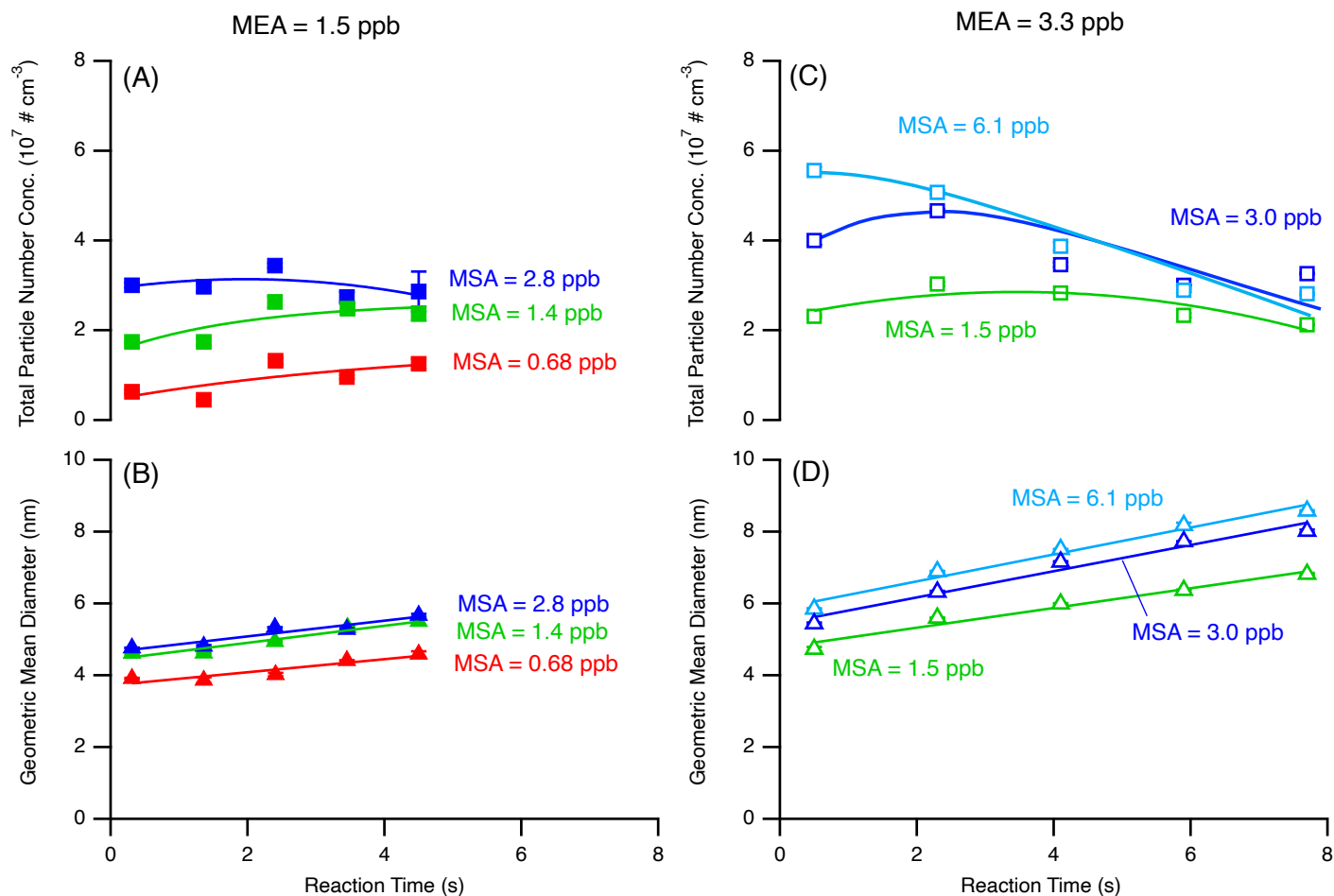**Summary of the SMPS measurements for the MSA+MEA reaction system**

Figure S12. Evolution of the particle total number concentrations and geometric mean diameters observed for the MSA+MEA reaction as a function of the reaction time in the flow reactor. In panels (A) and (C), the lines are guides to the eye, while in panels (B) and (D), the lines are linear fits to the data. All data represent replicate scans (n = 5) and are displayed with one standard deviation. Corresponding size distributions are given in Fig. 1. All measurements were corrected for the losses in the sampling lines.

Influence of relative humidity on the particles formed from the MSA+MEA reaction
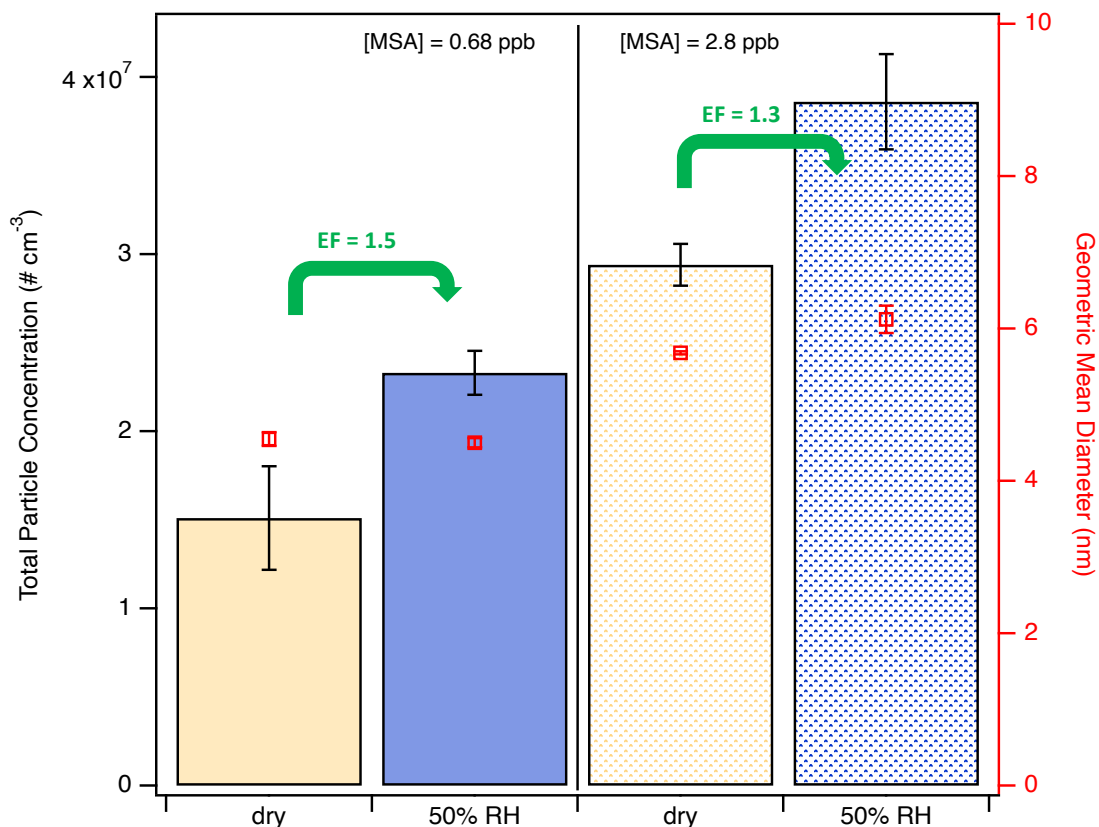

Figure S13. Comparison of the total number concentration (left axis) measured in the MSA+MEA system under either dry conditions (yellow) or in the presence of water vapor corresponding to 50% relative humidity (blue). For all conditions, the MEA concentration is 1.5 ppb. The data for each condition represent the average over 2-5 experiments with the error bar representing one standard variation. Red data points correspond to the averaged geometric mean diameter (right axis) for each condition (± one standard deviation). All measurements were performed at 4.5 s reaction time and were corrected for particle losses through the sampling lines.
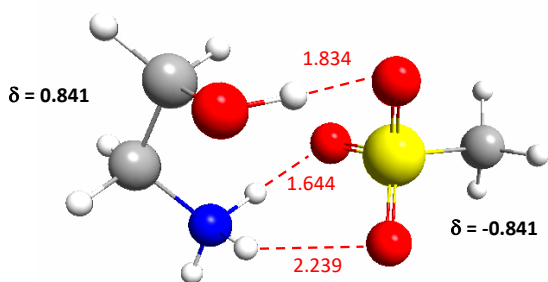
Structures, key geometrical parameters (in angstroms), particle charges (in atomic units) and dissociation energies of the most stable MSA-MEA cluster structures
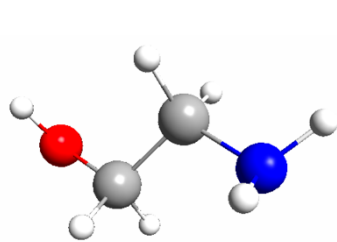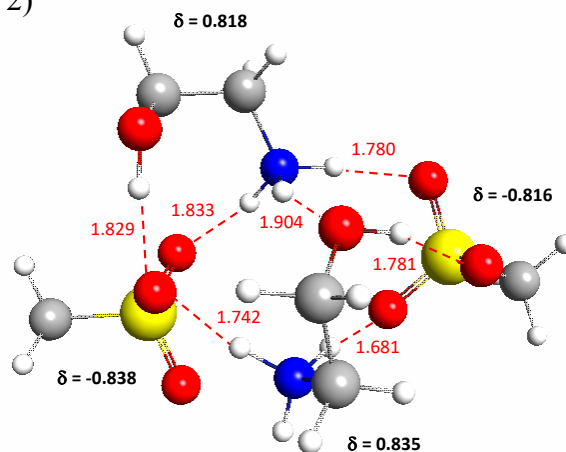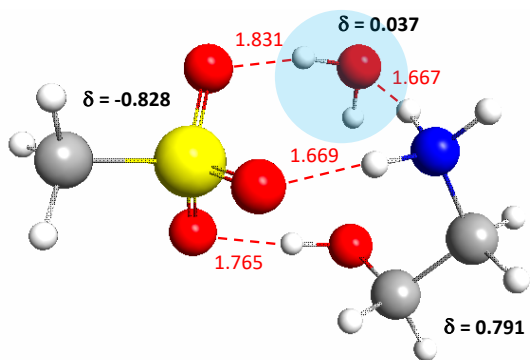

MEA (structure 1)
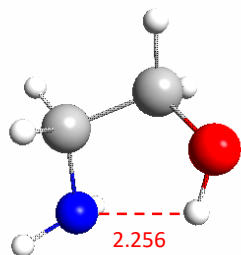
MEA (structure 2)
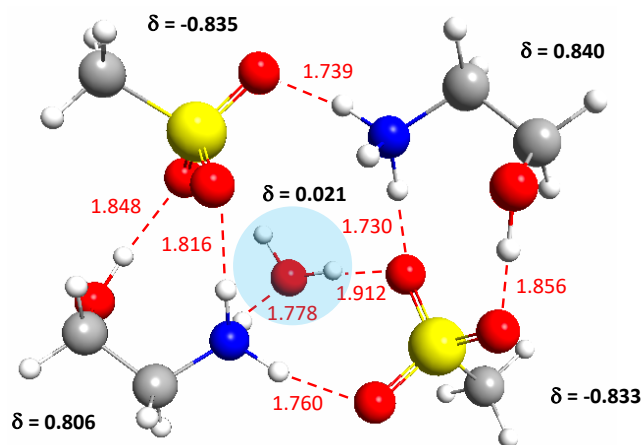
MSA-MEA
ΔE_{diss} = 24.1 kcal/mol

2MSA-2MEA
ΔE_{diss} = 85.5 kcal/mol

MSA-MEA-H_2O
ΔE_{diss} = 41.6 kcal/mol
$\Delta E_{dehydration}$ = 17.5 kcal/mol

2MSA-2MEA-H_2O
ΔE_{diss} = 99.7 kcal/mol
$\Delta E_{dehydration}$ = 14.2 kcal/mol

Figure S14. Structures, key geometrical parameters including bond length (in angstroms), partial charges (δ; in atomic units) and dissociation energies of the most stable MSA-MEA cluster structures. The initial lowest energy cluster structures were taken from Shen et al.[9] and recalculated using the QChem 4.3 program package[10] using density functional theory (DFT) with the B3LYP hybrid functional[11] and the 6-31+G(d) basis set. Additionally, the DFT-D3(0) dispersion correction from Grimme was used.[12] In this paper, the abbreviation B3LYP-D3/6-31+G(d) is used for this level of theory. Our previous studies showed that this method gives reasonable predictions for geometry and structure, vibrational frequencies, energies, enthalpies, and Gibbs free energies for the MSA-amines clusters.[13-16] Partial charges were calculated at the B3LYP-D3/6-31+G(d) level using natural bond orbital (NBO) analysis.[17,18] All computed energies have been corrected for the zero point energies. Dissociation energies were calculated for the complete dissociation to starting monomers or for the dehydration reaction. Calculations were conducted to illustrate the amount of coordination between molecules inside the MSA-MEA clusters. In all the clusters, the MEA molecule adopts a gauche conformation (structure 2), where the -OH group is facing the -NH_2 group, which is lower in energy by 3.28 kcal/mol compared to its other conformer (structure 1), consistent with previous studies.[19] Grey balls correspond to carbon atoms, white is for hydrogen atoms, yellow for sulfur atoms, red for oxygen atoms and blue for nitrogen atoms. Hydrogen bonds are labelled with dashed red lines, and the blue shaded circle highlights the one water molecule in the clusters.

Influence of relative humidity on the particles formed from the MSA+MA reaction
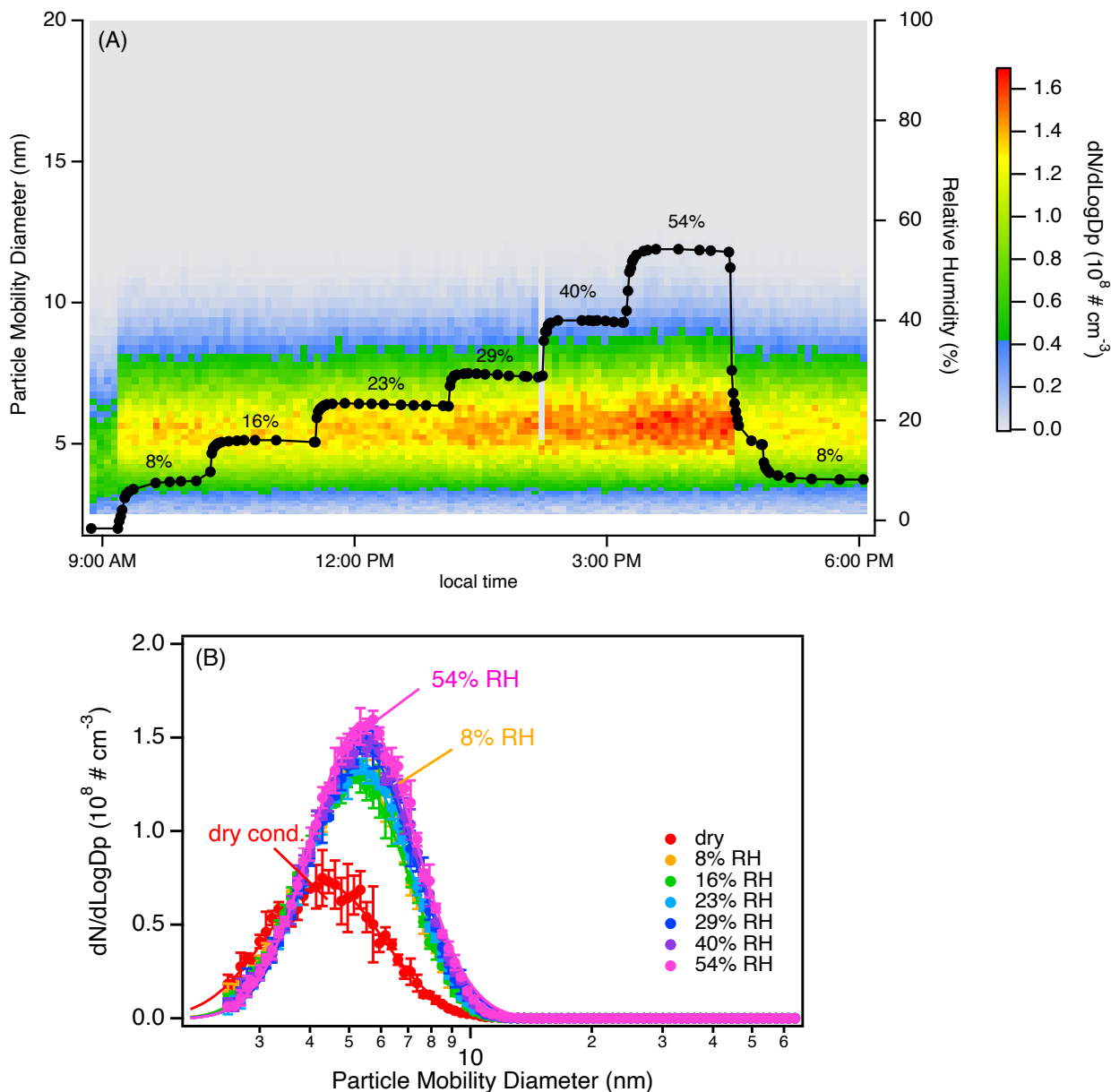

Figure S15. Evolution of the particle size distributions as a function of relative humidity (RH) from the reaction of MSA (1.4 ppb) with MA (10.8 ppb). Panel (A) represents the evolution as a function of time while panel (B) represents snapshots of the size distribution at a given RH (each distribution is an average of 5 replicate SMPS scans with the error bar representing one standard variation). All measurements were performed at 4.5 s reaction time. Particle size distributions were corrected for particle loss through the sampling lines.

References

1.   V. Perraud, X. X. Li, J. K. Jiang, B. J. Finlayson-Pitts, J. N. Smith, Size-resolved chemical composition of sub-20 nm particles from methanesulfonic acid reactions with methylamine and ammonia, *ACS Earth Space Chem.,* 2020, **4**, 1182-1194.
2.   M. L. Dawson, V. Perraud, A. Gomez, K. D. Arquero, M. J. Ezell, B. J. Finlayson-Pitts, Measurement of gas-phase ammonia and amines in air by collection onto an ion exchange resin and analysis by ion chromatography, *Atmos. Meas. Tech.,* 2014, **7**, 2733-2744.
3.   S.-L. von der Weiden, F. Drewnick, S. Borrmann, Particle loss calculator - A new software tool for the assessment of the performace of aerosol inlet systems, *Atmos. Meas. Tech.,* 2009, **2**, 469-494.
4.   J. N. Smith, K. F. Moore, P. H. McMurry, F. L. Eisele, Atmospheric measurements of sub-20 nm diameter particle chemical composition by thermal desorption chemical ionization mass spectrometry, *Aerosol Sci. Technol.,* 2004, **38**, 100-110.
5.   H. Chen, S. Chee, M. J. Lawler, K. C. Barsanti, B. M. Wong, J. N. Smith, Size resolved chemical composition of nanoparticles from reactions of sulfuric acid with ammonia and dimethylamine, *Aerosol Sci. Technol.,* 2018, **52**, 1120-1133.
6.   M. J. Lawler, P. M. Winkler, J. Kim, L. Ahlm, J. Trostl, A. P. Praplan, S. Schobesberger, A. Kuerten, J. Kirkby, F. Bianchi, J. Duplissy, A. Hansel, T. Jokinen, H. Keskinen, K. Lehtipalo, M. Leiminger, T. Petaja, M. Rissanen, L. Rondo, M. Simon, M. Sipila, C. Williamson, D. Wimmer, I. Riipinen, A. Virtanen, J. N. Smith, Unexpectedly acidic nanoparticles formed in dimethylamine-ammonia-sulfuric-acid nucleation experiments at CLOUD, *Atmos. Chem. Phys.,* 2016, **16**, 13601-13618.
7.   J. K. Jiang, C. M. Kim, X. L. Wang, M. R. Stolzenburg, S. L. Kaufman, C. L. Qi, G. J. Sem, H. Sakurai, N. Hama, P. H. McMurry, Aerosol charge fractions downstream of six bipolar chargers: effects of ion source, source activity, and flowrate, *Aerosol Sci. Technol.,* 2014, **48**, 1207-1216.
8.   V. Perraud, J. Olfert, J. N. Smith, Effective density measurement of sodium methanesulfonate and aminium chloride nanoparticles, *Aerosol Sci. Technol.,* 2022, **57**, 355-366.
9.   J. Shen, H.-B. Xie, J. Elm, F. Ma, J. Chen, H. Vehkamaki, Methanesulfonic acid-driven new particle formation enhanced by monoethanolamine: A computational study, *Environ. Sci. Technol.,* 2019, **53**, 14387-14397.
10. Y. H. Shao, Z. T. Gan, E. Epifanovsky, A. T. B. Gilbert, M. Wormit, J. Kussmann, A. W. Lange, A. Behn, J. Deng, X. T. Feng, D. Ghosh, M. Goldey, P. R. Horn, L. D. Jacobson, I. Kaliman, R. Z. Khaliullin, T. Kus, A. Landau, J. Liu, E. I. Proynov, Y. M. Rhee, R. M. Richard, M. A. Rohrdanz, R. P. Steele, E. J. Sundstrom, H. L. Woodcock, P. M. Zimmerman, D. Zuev, B. Albrecht, E. Alguire, B. Austin, G. J. O. Beran, Y. A. Bernard, E. Berquist, K. Brandhorst, K. B. Bravaya, S. T. Brown, D. Casanova, C. M. Chang, Y. Q. Chen, S. H. Chien, K. D. Closser, D. L. Crittenden, M. Diedenhofen, R. A. DiStasio, H. Do, A. D. Dutoi, R. G. Edgar, S. Fatehi, L. Fusti-Molnar, A. Ghysels, A. Golubeva-Zadorozhnaya, J. Gomes, M. W. D. Hanson-Heine, P. H. P. Harbach, A. W. Hauser, E. G. Hohenstein, Z. C. Holden, T. C. Jagau, H. J. Ji, B. Kaduk, K. Khistyaev, J. Kim, J.

Kim, R. A. King, P. Klunzinger, D. Kosenkov, T. Kowalczyk, C. M. Krauter, K. U. Lao, A. D. Laurent, K. V. Lawler, S. V. Levchenko, C. Y. Lin, F. Liu, E. Livshits, R. C. Lochan, A. Luenser, P. Manohar, S. F. Manzer, S. P. Mao, N. Mardirossian, A. V. Marenich, S. A. Maurer, N. J. Mayhall, E. Neuscamman, C. M. Oana, R. Olivares-Amaya, D. P. O'Neill, J. A. Parkhill, T. M. Perrine, R. Peverati, A. Prociuk, D. R. Rehn, E. Rosta, N. J. Russ, S. M. Sharada, S. Sharma, D. W. Small, A. Sodt, T. Stein, D. Stück, Y. C. Su, A. J. W. Thom, T. Tsuchimochi, V. Vanovschi, L. Vogt, O. Vydrov, T. Wang, M. A. Watson, J. Wenzel, A. White, C. F. Williams, J. Yang, S. Yeganeh, S. R. Yost, Z. Q. You, I. Y. Zhang, X. Zhang, Y. Zhao, B. R. Brooks, G. K. L. Chan, D. M. Chipman, C. J. Cramer, W. A. Goddard, M. S. Gordon, W. J. Hehre, A. Klamt, H. F. Schaefer, M. W. Schmidt, C. D. Sherrill, D. G. Truhlar, A. Warshel, X. Xu, A. Aspuru-Guzik, R. Baer, A. T. Bell, N. A. Besley, J. D. Chai, A. Dreuw, B. D. Dunietz, T. R. Furlani, S. R. Gwaltney, C. P. Hsu, Y. S. Jung, J. Kong, D. S. Lambrecht, W. Z. Liang, C. Ochsenfeld, V. A. Rassolov, L. V. Slipchenko, J. E. Subotnik, T. Van Voorhis, J. M. Herbert, A. I. Krylov, P. M. W. Gill, M. Head-Gordon, Advances in molecular quantum chemistry contained in the Q-Chem 4 program package, *Mol. Phys.,* 2015, **113**, 184-215.

11.   A. D. Becke, Density-Functional Thermochemistry .3. The Role of Exact Exchange, *J. Chem. Phys.,* 1993, **98**, 5648-5652.

12.   S. Grimme, J. Antony, S. Ehrlich, H. Kried, A consistent and accurate ab initio parametrization of density functional dispersion correction (DFT-D) for the 94 elements H-Pu, *J. Chem. Phys.,* 2010, **132**, Art No 154104 (154101-154119).

13.   J. Xu, V. Perraud, B. J. Finlayson-Pitts, R. B. Gerber, Uptake of water by an acid-base nanoparticle: theoretical and experimental studies of the methanesulfonic acid-methylamine system, *Phys. Chem. Chem. Phys.,* 2018, **20**, 22249-22259.

14.   J. Xu, B. J. Finlayson-Pitts, R. B. Gerber, Proton transfer in mixed clusters of methanesulfonic acid, methylamine, and oxalic acid: implications for atmospheric particle formation, *J. Phys. Chem. A,* 2017, **121**, 2377-2385.

15.   H. Chen, M. E. Varner, R. B. Gerber, B. J. Finlayson-Pitts, Reactions of methanesulfonic acid with amines and ammonia as a source of new particles in air, *J. Phys. Chem. B,* 2016, **120**, 1526-1536.

16.   M. L. Dawson, M. E. Varner, V. Perraud, M. J. Ezell, R. B. Gerber, B. J. Finlayson-Pitts, Simplified mechanism for new particle formation from methanesulfonic acid, amines, and water via experiments and ab initio calculations, *Proc. Natl. Acad. Sci. USA,* 2012, **109**, 18719-18724.

17.   J. P. Foster, F. Weinhold, Natural hybrid orbitals, *J. Am. Chem. Soc.,* 1980, **102**, 7211-7218.

18.   A. E. Reed, F. Weinhold, Natural bond orbital analysis of nearHartree-Fock water dimer, *J. Chem. Phys.,* 1983, **78**, 4066-4073.

19.   C. F. P. Silva, M. L. T. S. Duarte, R. Fausto, A concerted SCF-MO ab initio and vibrational spectroscopic study of the conformational isomerism in 2-aminoethanol, *J. Mol. Struct.,* 1999, **482**, 591-599.